A Finite Element Investigation of Elastic Flow Asymmetries in Cross-Slot Geometries Using a Direct Steady Solver

A. Filali[1], L. Khezzar[1,2]

Abstract: Numerical investigations of purely-elastic instabilities occurring in creeping flows are reported in planar cross-slot geometries with both sharp and round corners. The fluid is described by the upper-convected Maxwell model, and the governing equations are solved using the finite element technique based on a steady (non-iterative) direct solver implemented in the POLYFLOW commercial software (version 14.0). Specifically, extensive simulations were carried out on different meshes, with and without the use of flow perturbations, for a wide range of rheological parameters. Such simulations show the onset of flow asymmetries above a critical Deborah number (De). The effect of rounding the corners is also addressed. The numerical results obtained are found to be in good quantitative agreement with previously published numerical results

1 Introduction

The cross-slot flow belongs to the group of stagnation point flows and in this particular case the stagnation point is created at the center. [Arratia et al (2006)] have reported experimentally symmetry-breaking and oscillatory instabilities in cross-slot flows of polymer solutions at high enough Deborah (De) numbers. Here De is defined as ($\equiv \lambda U/H$) and represents the ratio of a fluid characteristic time (relaxation time, λ) to that of the flow with U and H representing a characteristic velocity and length scales respectively. Additionally, the cross-slot geometry has been a widely employed extensional flow test case in computational rheology [Remmelgas et al (1999); Singh and Leal (1995)]. In particular, the flow in such geometry is characterized by a strong extensional component similar to that found in several industrial

---

[1] Department of Mechanical Engineering, Petroleum Institute, Abu Dhabi, United Arab Emirates.
[2] Corresponding author. Email: lkhezzar@pi.ac.ae

flows and in a number of practical applications such as in flow focusing devices for the generation of droplets [Anna et al (2003)], in DNA sequencing [Dylla-Spears et al (2010)], in extensional flow oscillatory rheometry [Odell and Carrington (2006)] and in an extensional micro-rheometer [Haward (2012)]. Hence, the ability to predict the details of such flows and the symmetry breakdown not only provides a good test of the computational techniques that can be used in the design of practical equipment where similar flows can occur, but is also an essential requirement for the correct design of microsystems. In fact, the onset of flow instabilities limits the range of operation of the cross-slot device as an extensional rheometer, or as a component of a flow focusing device for the generation of droplets. In contrast, flow instabilities may also be desired at microscale for development of efficient micromixing systems.

Contrary to Newtonian fluid flows that become unstable only at relatively high Reynolds numbers (Re), flows of viscoelastic fluids such as polymer solutions and melts, are known to exhibit flow instabilities and nonlinear dynamical behavior at extremely low Re, defined as Re ($\equiv \rho UH/\eta$) and represents the relative importance of inertia to viscous forces within the flow, ρ and η represent the density and the viscosity of the fluid respectively. Such instabilities are due to nonlinear elastic effects and can be seen in many practical applications such as in the rheometry of complex fluids. In shear, for example, [Giesekus (1966)] observed cellular instabilities in Taylor-Couette flows of non-Newtonian fluids at very low Reynolds (Taylor) numbers and [Larson et al (1990)] demonstrated experimentally that such non-Newtonian instabilities are caused by fluid elasticity. The mechanism of this instability is a purely elastic one, and is related to the coupling of perturbations in the hoop stress with the base state velocity gradients.

The elastic instabilities are also often present in extensionally dominated non-Newtonian fluid flows exhibiting an interior stagnation point and in this respect the cross-slot geometry has recently been the focus of several identifications. [Arratia et al (2006)] identified experimentally, using particle tracking image velocimetry and flow visualization, a new type of flow instability associated with viscoelasticity, for the flow in a microscale cross-slot geometry. Two distinct instabilities were identified in the low Re (< 0.01) flow of flexible polymer solutions: the first above a critical flow rate (or Deborah number), where the flow patterns progressively acquired a steady flow asymmetry in a symmetric geometry, followed by a second instability towards time-dependent asymmetric flows above a second (higher) critical Deborah number.

Numerical investigations of the two-dimensional cross-slot flow, using the finite-volume methodology were carried by [Poole et al (2007)], who showed that the same asymmetric behavior can be predicted using the Upper-Convected Maxwell

(UCM) model and were able to capture qualitatively the supercritical bifurcation, under creeping-flow conditions. At low Deborah numbers the flow remains steady and symmetric, whereas above a critical Deborah number (De_{cr} = 0.31) the flow becomes asymmetric but remains steady. Increasing further the Deborah number produced a second instability where the flow became time-dependent. It was also shown that increasing the Reynolds number leads to a shift of the first critical Deborah number to higher values, and a considerable decrease of the flow asymmetry. The authors conjectured that the asymmetry is due to the compressive nature of the flow upstream of the stagnation point. [Oliveira et al (2009)], using a finite-volume code and both UCM and Phan-Thien–Tanner (PTT) models, considered a cross-slot with three inlets and one exit arm and found the two types of instability mentioned above in this flow focusing device. The authors conjectured also that this bifurcation to asymmetric flow is a stress relief mechanism. A simulation of a three-dimensional cross-slot geometry with six arms was carried out by [Afonso et al (2010)] using the UCM model. The influences of the ratio of the inlet to the outlet flow rates and of the Deborah and Reynolds numbers for different types of extensional flow corresponding to biaxial and uniaxial extensional flow configurations were analyzed. For the uniaxial extensional flow the authors reported similar findings to the 2D planar flow geometry where the flow becomes steady asymmetric for the first critical Deborah number, $De_{cr} \approx 0.22$ and unsteady asymmetric for a second critical Deborah number, $De_{cr} \approx 0.32$. However, for the biaxial flow configuration only one transition from steady symmetric to unsteady asymmetric flow was observed, at $De \approx 0.61$. It was also shown for the uniaxial flow configuration that inertia has a stabilizing effect and the first critical Deborah number increases with *Re*, while for the second transition inertia helps destabilize the flow and the second critical Deborah number decreases with *Re*. This role of inertia is similar to that previously seen for the 2D crossslot flow by [Poole et al (2007)].

Subsequently, other numerical studies analyzed the influence of the constitutive equation and its rheological parameters such as [Rocha et al (2009)], who used the shear-thinning FENE-P model [Bird et al (1980); Bird et al (1987)] and the constant-viscosity FENE-CR model proposed by [Chilcott and Rallison (1988)], respectively. It is clear from the above that purely elastic instabilities in cross-slot flows have been identified using experimental and numerical means and that both approaches show that the symmetry to asymmetry steady flow transition is a supercritical bifurcation with the correct signature (bifurcation diagram). However and understandably, the rheology of the fluids used in the simulations have not attempted to faithfully reproduce the actual fluids used in the experiments which could explain the discrepancies between the values of the critical Deborah numbers from the calculations and experiments. Most simulations referred to for the

viscoelastic flow in the cross-slot made use of the finite volume technique based on a variety of iterative solvers either in steady or unsteady modes and represent contributions from essentially one group of researchers using the same viscoelastic flow solver, hence it remains to be shown whether the bifurcation can be detected by other integration techniques as well. Thus, in this work we investigate the viscoelastic flow in 2D orthogonal geometries with four arms, consisting of two opposed inlets and outlets, using the UCM model at low Reynolds number ($Re \approx 0$). The numerical integration approach uses for the first time the finite element technique embedded in the POLYFLOW commercial software, which is based on the DEVSS/SU (Discrete Elastic Viscous Split Stress/Streamline Upwinding) scheme and contrary to previous works we use a non-iterative direct robust solver. In this work and because a non-iterative direct solver is used we show that the supercritical bifurcation can still be obtained using a non-symmetrical mesh. The parameters that influence the appearance of asymmetric flow such as the roundness of the corners are discussed and confirm previously obtained results.

2   Mathematical and numerical models

The basic equations governing the viscoelastic incompressible flow of a UCM fluid are the mass conservation and the momentum equations, together with a constitutive equation for the upper-convected Maxwell model, which are given by

$$\nabla \cdot \boldsymbol{u} = 0, \tag{1}$$

$$\rho \nabla \cdot (\boldsymbol{uu}) = -\nabla p + \nabla \cdot \boldsymbol{T} \tag{2}$$

$$\boldsymbol{T} + \lambda \stackrel{\nabla}{\boldsymbol{T}} = 2\eta \boldsymbol{D}, \tag{3}$$

where $\boldsymbol{u}$ represents the velocity, p the pressure, ρ the fluid density, $\boldsymbol{T}$ the extra-stress tensor, $\boldsymbol{D}$ the rate of deformation tensor, η is the viscosity coefficient of the UCM model and λ is the relaxation time of the fluid. The UCM constitutive equation is the simplest model that features memory effects and elastic normal stresses and is characterized by a constant shear viscosity. These are some of the characteristics of a class of real viscoelastic fluids, the so-called Boger fluids, but at the same time this constitutive model can exhibit unbounded stresses in pure extensional flow leading to convergence difficulties of the numerical methods, so it is used as an important test for the performance of codes in benchmark flows in computational rheology.

The upper-convected derivative $\stackrel{\nabla}{\boldsymbol{T}}$ of the viscoelastic extra-stress and the rate of deformation tensor $\boldsymbol{D}$ are defined respectively by

$$\stackrel{\nabla}{\boldsymbol{T}} = \boldsymbol{u} \cdot \nabla \boldsymbol{T} - \boldsymbol{T} \cdot \nabla \boldsymbol{u} - \nabla \boldsymbol{u}^T \cdot \boldsymbol{T}, \tag{4}$$

$$\boldsymbol{D} = (\nabla \boldsymbol{u} + \nabla \boldsymbol{u}^T)/2. \tag{5}$$

In view of its rheological simplicity, the UCM model is one of the simplest viscoelastic constitutive equations. It exhibits a constant shear viscosity and a quadratic first normal-stress difference as a function of the shear rate. It is however, recommended only when limited information about the fluid is available, or when a qualitative prediction is sufficient. Nevertheless, this model is very challenging from the numerical point of view, due to its inherent stress singular behavior near corners or near geometric singularities [Oliveira et al 1998]). The loss of convergence of the iterative schemes beyond a critical high Weissenberg number in a contraction flow [Keunings (1986)], often accompanied by a loss of evolution of the configuration tensor [Dupret and Marchal (1986)] were major motivations for developments in computational rheology.

In this work, the numerical simulations have been performed using the POLYFLOW solver, which is based on the finite element numerical method. The advective nature of the constitutive equation and the interaction of multiple discrete unknown fields (viscoelastic stress, velocity and pressure) both present a challenge to numerical modeling. An algebraic multi-frontal Approximate Minimum Fill (AMF) direct solver is used to solve the governing equations. Due to the highly non-linear characteristics of non-Newtonian flows, their numerical simulation remains a challenging task in terms of accuracy, stability and convergence. To deal with convergence and obtain stable solutions, a mixed finite element method (DEVSS/SU), which combines the discrete version of the elastic-viscous split stress (DEVSS) method, [Guénette and Fortin (1995)], and the streamline upwinding (SU) scheme, was used for discretizing the governing equations.

The DEVSS method is proposed as a discrete version of the elastic viscous stress splitting method (EVSS) of [Rajagopalan et al (1990)], in which an auxiliary variable $\underline{\boldsymbol{D}}$, as a discrete counterpart of the rate of deformation tensor and an independent variable is introduced, and determined in terms of satisfaction in a weighted average form,

$$\underline{\boldsymbol{D}} - \boldsymbol{D} = \boldsymbol{0}. \tag{6}$$

Further, taking the divergence of Eq. (5) and adding a diffusive term $-2\eta\nabla \cdot (\underline{\boldsymbol{D}} - \boldsymbol{D})$ to the momentum equation, with the use of Eq. (4), we obtain

$$\rho\nabla \cdot (\boldsymbol{uu}) = -\nabla p + 2\eta\nabla \cdot \boldsymbol{D} + \nabla \cdot \boldsymbol{T} - 2\eta\nabla \cdot \underline{\boldsymbol{D}}. \tag{7}$$

This equation is the stabilized form of the original momentum equation re-formulated in terms of the DEVSS method. Equations (1), (3) and (7) constitute the governing equations, in which the three main variables $\boldsymbol{u}$, p, $\boldsymbol{T}$ and an auxiliary variable $\underline{\boldsymbol{D}}$

are involved. $\underline{\boldsymbol{D}}$ is the projected rate-of-deformation tensor into the stress space [Rajagopalan et al (1990)].

In the present study, an evolution method for the relaxation time λ and the DE-VSS/SU method were used to reach numerical convergence and to deal with the viscoelastic stress terms. In POLYFLOW, convergence assessment is based on the calculation of a global relative error for each field (pressure, velocity, extra-stress). The relative error is calculated as the ratio of the difference in the value of a given field at every node between two successive iterations and the maximum value of the field. The convergence criterion used in our simulations was 10^{-5}, which is considered to be sufficient for a properly converged solution.

Most non-linear problems require successive incrementation (or decrementation) of the parameters controlling the non-linearity. Each iterative step starts from the solution obtained at the previous step, or from a solution extrapolated on the basis of previous solutions. Evolution is an incremental numerical scheme facilitating the convergence of complex flow problems. In POLYFLOW, any problem parameter can be defined as an algebraic function of the single evolution variable S. During the evolution process, the value of the specific parameter will be calculated as the product of its nominal value and of a function of S selected for that particular parameter.

For differential type viscoelastic constitutive models the appropriate evolution is usually based on either the fluid relaxation time (λ) or the flow rate Q providing gradual increases in the values assigned to the Deborah number. In this work the evolution technique is applied to the relaxation time such that $\lambda_i = f(S_i)\,\lambda_{nom}$, where λ_{nom} is the nominal relaxation time, $f(S_i) = S_i = S_{i-1} + \Delta S_{i-1}$, with initial and final values of S given by $S_0 = 0$ and $S_{final} = 1$, respectively. The initial value of ΔS is $\Delta S_0 = 0.01$, with S representing the evolution variable.

The solution of the non-linear problem is obtained using a direct solver based on Gaussian elimination with the converged solution of the previous step used as the initial guess when available. For example, for $i = 1$, we have $\lambda_1 = f(S_1)\,\lambda_{nom}$, if the solution converges $\Delta S_1 = 1.5\,\Delta S_0$ and $S_2 = S_1 + \Delta S_1$, then for $i = 2$, $\lambda_2 = f(S_2)\,\lambda_{nom}$. However, if the solution diverges, $\Delta S'_1 = \Delta S_1 / 2$ and $S_2 = S_1 + \Delta S'_1$ and the iteration is re-done. If the solution diverges again ΔS_i is progressively halved until it becomes less than a minimum $\Delta S_{min} = 10^{-4}$ at which point the simulation is interrupted.

3   Problem geometry and setup

The cross-slot geometries are shown schematically in Figure 1 for the cases with (a) sharp and (b) round corners, the latter with a radius of curvature $R = 0.1H$. All

branches have the same width (H) and the inlet and outlet branches have lengths of ten channel widths ($10\,H$). The geometry is two-dimensional and symmetric about the planes $x = 0$ and $y = 0$, with the origin of the coordinates system set at the center of the geometry. At the inlets fully-developed velocity and stress profiles are imposed (in some tests uniform velocity profiles were also used) and the chosen inlet length is more than sufficient for the flow at the junction to be independent of the inlet condition. Similarly, the outlets are sufficiently long to avoid any effect of the outflow boundary condition upon the flow in the central region. At the outlet planes vanishing axial gradients are applied to velocity, extra-stress and pressure gradient (Neumann boundary conditions: $\partial\varphi/\partial y = 0$), and no-slip conditions are imposed at all channel walls.
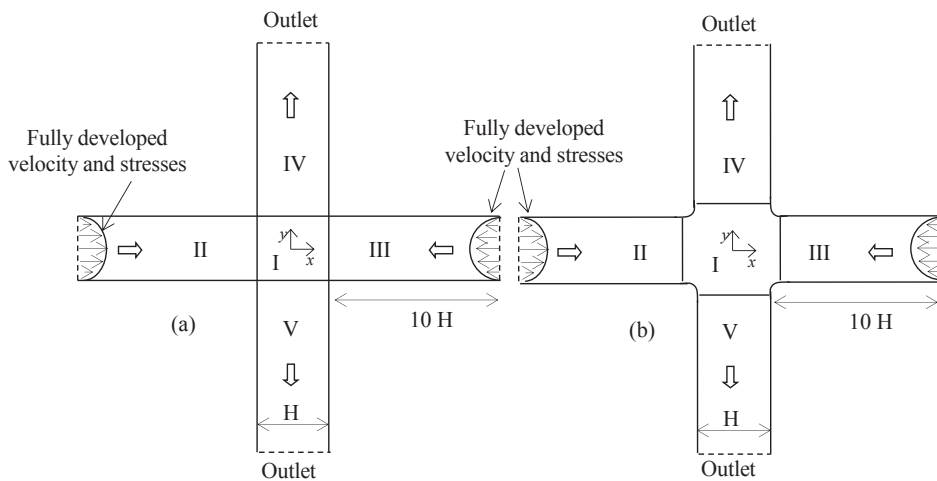
Figure 1: Schematic of cross-slot geometry: (a) Sharp corners; (b) Round corners.

Grid sensitivity tests have been conducted with different numbers of cells to calculate the velocity profile at the center of the cross-slot and obtain a grid independent solution. Details of the different grid sensitivity tests performed are given in Tables 1 and 2 for the sharp and round corners cross-slot geometries, respectively.

The finite element grid in Figure 2 was established based on the expected behavior of the solution. Near the walls the gradients produced by the no-slip boundary condition dictated the use of smaller mesh spacing than for the slowly varying core flow regions. The gradients produced by the sharp and round corners in the central square also required a refined mesh to represent the solution adequately.

The variation of normalized streamwise velocity profile along the inlet centerline is plotted for different meshes in Figure 3 (a) and (b) for the sharp and round corners

Table 1: Characteristics of the mesh for sharp corners geometry

Blocks	M1		M2		M3	
	Nx	Ny	Nx	Ny	Nx	Ny
I	25	25	50	50	75	75
II	105	25	130	50	180	75
III	105	25	130	50	180	75
IV	25	105	50	130	75	180
V	25	105	50	130	75	180
TNE =	10125		28500		56625	
TNC =	10556		29121		57456	

Table 2: Characteristics of the mesh for round corners geometry

Blocks	M4		M5		M6	
	N1	N2	N1	N2	N1	N2
I	10	12	15	25	25	35
	Nx	Ny	Nx	Ny	Nx	Ny
II	105	25	130	50	180	75
III	105	25	130	50	180	75
IV	25	105	50	130	75	180
V	25	105	50	130	75	180
TNE =	10560		28000		50400	
TNC =	11049		28661		51261	
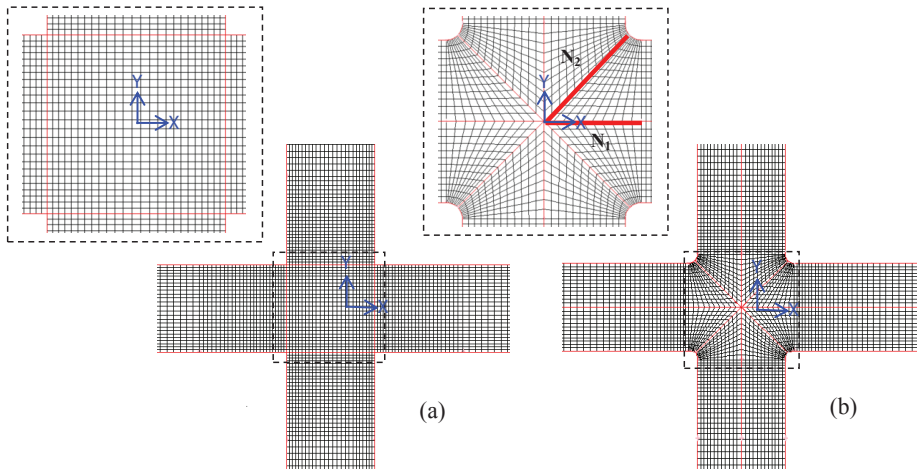
Figure 2: Details of symmetric meshes (-2.5 ≤ *x/H* ≤ 2.5, -2.5 ≤ *y/H* ≤ 2.5): (a) Sharp corners (Mesh M2); (b) Round corners geometry (Mesh M5).

cross-slot geometries, respectively. It is clear that the differences between meshes M2 and M3 for sharp corners and M5 and M6 for round corners geometry are negligible; therefore, to reduce the computational time further computations were carried out in meshes M2 and M5 for the sharp and round cross-slots, respectively.

It was found that the simulations with the symmetric meshes always returned a symmetric flow whatever the value of *De*. Consequently a mesh with a mild asymmetric distribution of cells was also used to see whether the calculated flow would become asymmetric as found by [Poole et al (2007)], where no perturbation was required to obtain the steady asymmetric flow using an iterative solver and a perfect symmetric mesh was considered in their study. Several meshes with different degrees of asymmetry were tried. Figure 4 represents the mesh with the mildest asymmetry that returned asymmetric flow beyond the critical *De*. Results with a higher asymmetry in the mesh were the same as the ones shown here. However, meshes with a lower asymmetry than Fig. 4 returned a symmetric flow throughout. The results of the extensive set of computations in both symmetric and asymmetric meshes are reported in the next section.

4   Results and discussion

The results presented in this section are mainly provided in the form of streamline patterns superimposed onto contour plots of the normalized first-normal stress dif-
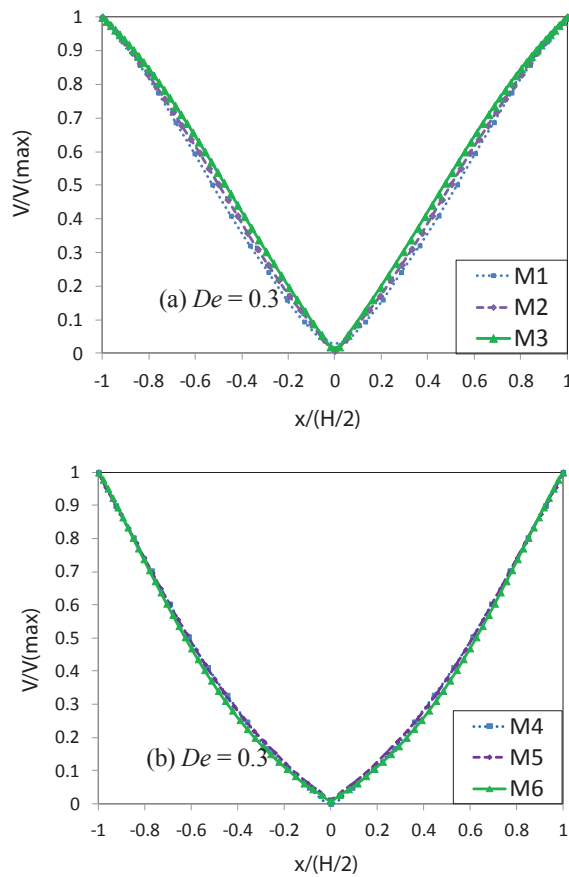
Figure 3: Dimensionless profiles of the streamwise velocity along the inlet center plane for different meshes: (a) Sharp corner (b) Round corner.

ference and in terms of the parameter DQ (which quantifies the flow asymmetry) as function of De, where $DQ = (Q_2-Q_1)/Q$ with $Q = Q_1 + Q_2 = UH$ representing the total flow rate per unit depth supplied to each inlet channel, which is divided in two partial flow rates Q_1 and Q_2 [Poole et al (2007)]. Symmetric and asymmetric flows are predicted for both geometries considered. The effects of the cross-slot sharp and round corners and of rheological parameters that influence the flow are discussed together with the effect of flow inertia.
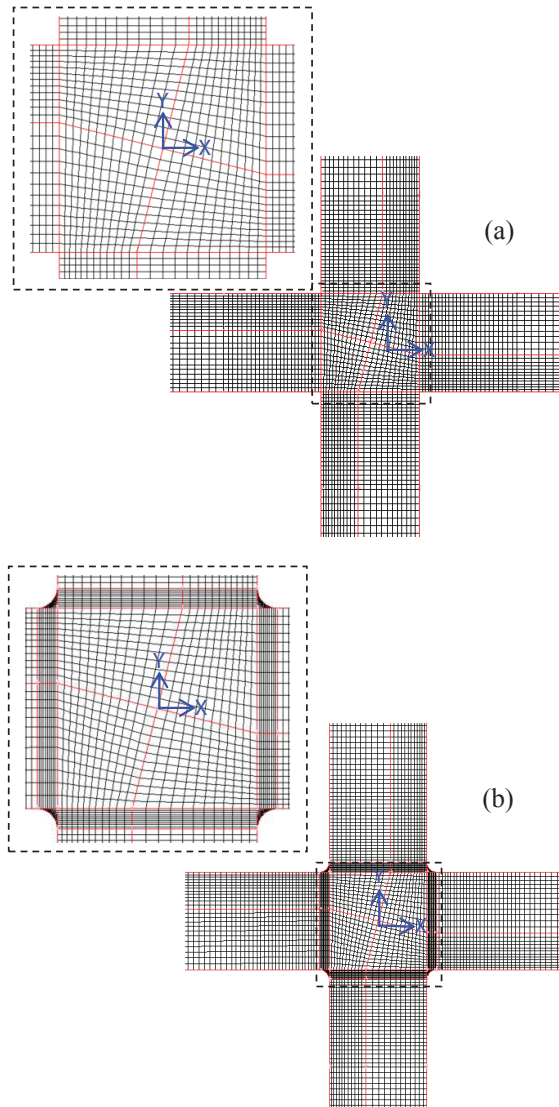
Figure 4: Details of asymmetric meshes near the intersection for the (a) sharp and (b) round corners geometries.

4.1   *Symmetric Flow*

Figures 5 and 6 present streamline patterns superimposed onto contour plots of $(\tau_{yy}-\tau_{xx})/(\eta\, U/H)$ for Newtonian and non-Newtonian fluids for both sharp and round corners geometries, respectively.
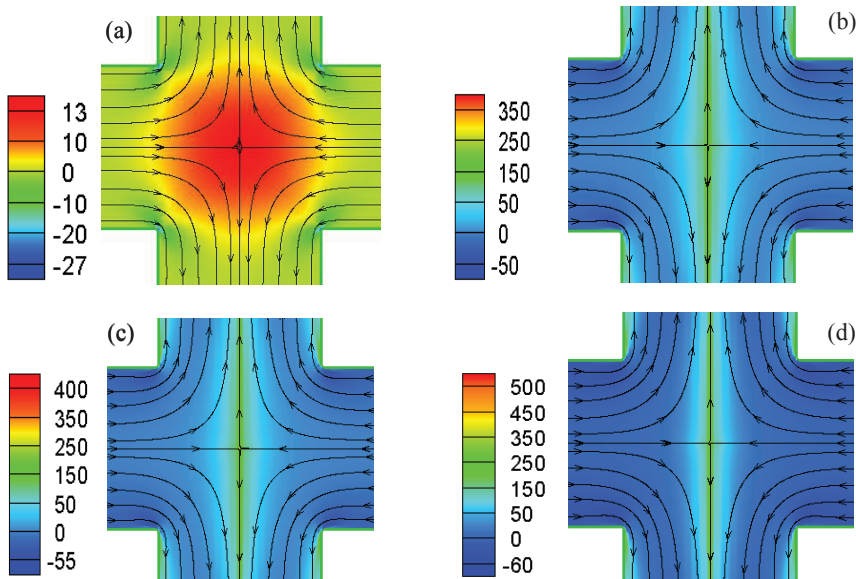
Figure 5: Streamline patterns superimposed onto dimensionless contour plots of $(\tau_{yy}-\tau_{xx})/(\eta U/H)$ for the sharp corner cross-slot mapped with a symmetric mesh: (a) De=0 (Newtonian); (b) $De = 0.34$; (c) $De = 0.38$; (d) $De = 0.45$.

For the sharp corner geometry, results for the Newtonian fluid presented in figure 5 (a) show a perfectly symmetric flow, as expected. For the non-Newtonian fluid at different supercritical Deborah numbers ($De = 0.34$, 0.38 and 0.45) the flow remains symmetric as shown in figures 5 (b), 5 (c) and 5 (d) respectively, even when the Deborah number exceeds the critical value computed by [Poole et al (2007)]. These cases were computed with symmetric meshes and it can be seen that the normalized normal stress difference values $(\tau_{yy}-\tau_{xx})/(\eta U/H)$ grow with Deborah number, but flow asymmetry is not captured even when using a highly refined mesh, such as M3.

Sharp corners are well known to be troublesome in the numerical solution of viscoelastic flow equations [Owens and Phillips (2002)] and in many of the early simulations of the cross-slot, in which only one quarter of the full geometry was
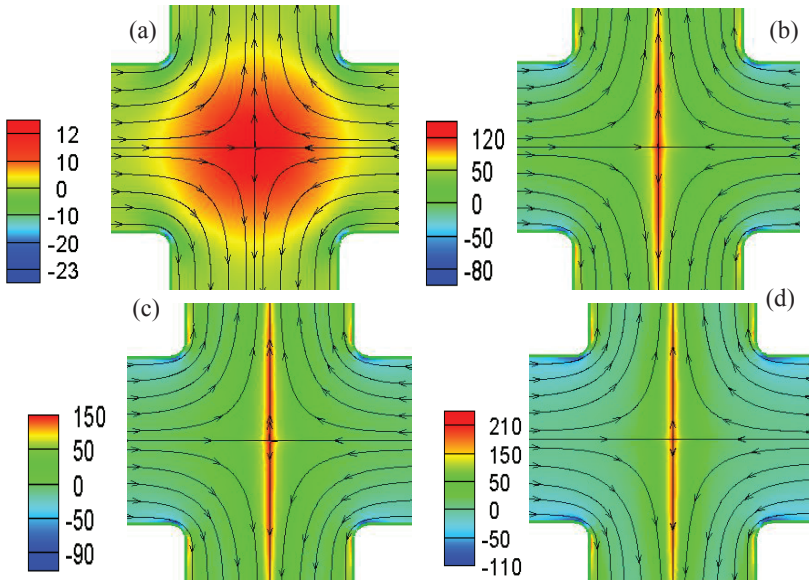
Figure 6: Streamlines patterns superimposed onto contour plots of $(\tau_{yy} - \tau_{xx})/(\eta U/H)$ for the round corner cross-slot mapped with a symmetric mesh: (a) *De*=0 (Newtonian); (b) *De* = 0.34; (c) *De* = 0.38; (d) *De* = 0.45.

simulated, the corner was artificially rounded off by a slight amount [Remmelgas (1999)] in order to enable high Deborah number solutions to be obtained. Computations were also carried out here in geometries with rounded corners and these are shown in Figure 6 for the same Deborah numbers of the sharp corner geometry. Again the flow is symmetric in this geometry mapped with symmetric meshes for all flows, i.e., for the Newtonian case as well as for the non-Newtonian flows at Deborah numbers of *De* = 0.34, 0.38 and 0.45. As will be shown later, the critical Deborah number for the round geometry is around 0.34, so the flows at the higher values of *De* are clearly supercritical and these symmetric flow solutions are a result of the non-iterative nature of the direct solver used

Bifurcation of the numerical solution is triggered by some possible imbalance of the high stresses generated in these corner regions and high compressive stresses generated along the centerline region of the two incoming flow streams. This behavior can be seen in the comparison between normalized stress difference values for the sharp corners geometry, which are larger than those of the round corners geometry for the same Deborah numbers, as is clear from the contour plots in Figures 5 and 6.

4.2   *Asymmetric Flow*

All simulations with a symmetric mesh returned a perfectly symmetric flow for the elastic fluids, even beyond the critical Deborah number determined by [Poole et al (2007)]. In addition, several tests with tighter convergence criteria equal to 10^{-10} also returned a perfectly symmetric flow beyond the critical Deborah number. Bearing in mind that the numerical approach uses a robust direct solver, it was decided to test separately two types of perturbations, one in terms of the inlet velocity at the initial stages of the computation and the second in the form of a slight asymmetry in the mesh topology used. This section reports on such calculations for both sharp and rounded corners.

Regarding the perturbation in the inlet velocity profile, two strategies were used to perform numerical simulations under conditions of supercritical *De*, but to no avail, i.e., the final solution was still a symmetric flow. In one case instead of using a uniform inlet velocity profile, an asymmetric inlet profile with the same bulk velocity was imposed at the beginning of the computations and after some iteration, the inlet profile was switched back to the uniform profile. In the other case the simulations were conducted under supercritical conditions only to converge to a solution that was symmetric. Then, on half of one inlet the velocity profile was increased by 10% (and 20% in a second trial) and on the other half the velocity profile was decreased by the same amount to preserve the bulk velocity. The numerical simulation was restarted for a while with this non-uniform inlet velocity profile, and subsequently restarted again with the original uniform profile until convergence. In all cases tested the final result was a symmetric flow. Next, the results obtained with the asymmetric mesh are discussed.

Streamlines superimposed on contours of the normalized first normal-stress difference $(\tau_{yy}\text{-}\tau_{xx})/(\eta\,U/H)$, are presented in Figure 7 for Newtonian and non-Newtonian fluid flows in the sharp corners cross-slot at increasing *De*, which were obtained with the asymmetric mesh of 10127 elements (10625 nodes) shown in Figure 4 (a). Using more refined asymmetric meshes, containing 30500 elements (31161 nodes) and 64000 elements (64881 nodes), led to divergence of the numerical method.

Using the asymmetric mesh of 10127 elements, perfectly symmetric flows were calculated for the Newtonian fluid and viscoelastic fluid at *De* = 0.28 as shown in Figures 7 (a) and 7 (b), respectively. Note that this Deborah number is below the critical value reported by [Poole et al (2007)], hence the results were expected. However, above a critical Deborah number of *De* ≈ 0.31, the flow becomes asymmetric and for higher Deborah numbers, such as *De* = 0.45, the flow is strongly asymmetric (cf. Figure 7 (f)). The corresponding local Weissenberg number ($Wi \equiv \lambda\dot{\varepsilon}$), based on the strain rate at the stagnation point, is also indicated
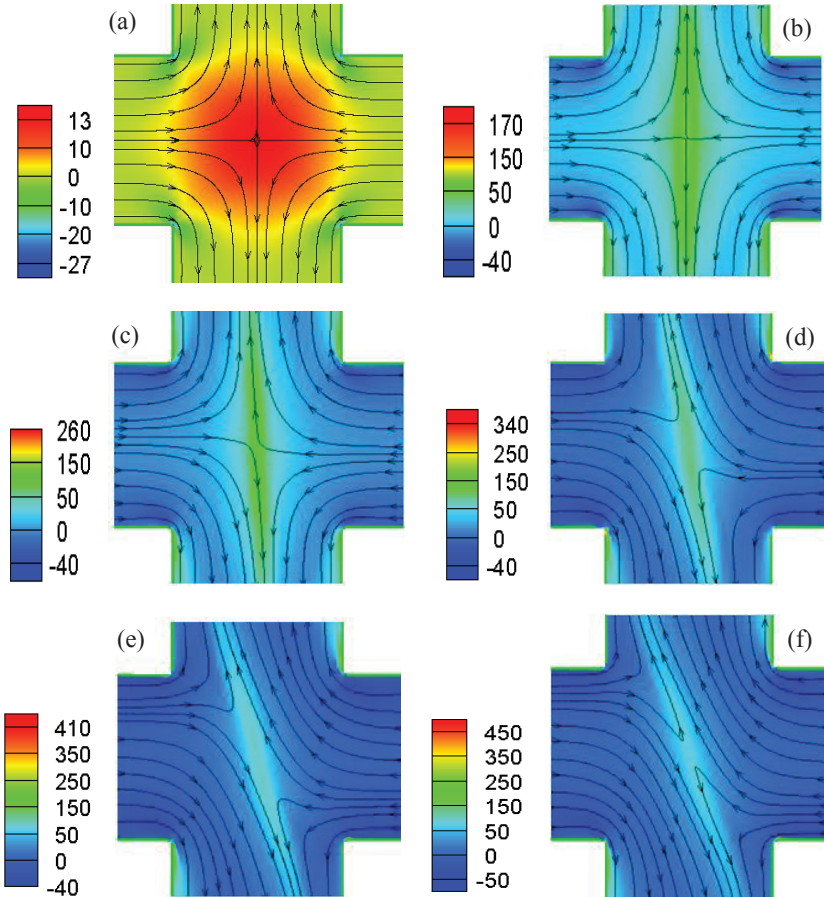
Figure 7: Streamlines patterns superimposed onto contour plots of $(\tau_{yy}-\tau_{xx})/(\eta U/H)$ for the sharp corner cross-slot mapped with an asymmetric mesh: (a) $De = 0$ (Newtonian); (b) $De = 0.28$ ($Wi = 0.554$); (c) $De = 0.31$ ($Wi = 0.566$); (d) $De = 0.34$ ($Wi = 0.527$); (e) $De = 0.39$ ($Wi = 0.485$); (f) $De = 0.45$ ($Wi = 0.434$).

in figure 7.

The non-dimensional parameter DQ is used to quantify the degree of flow asymmetry and is presented in Figure 8. The comparison in Figure 8(a) between the present work and the numerical results of [Poole et al (2007)] for the variation of DQ with the Deborah number, shows a good agreement for De varying from 0.25 to 0.45, which is the maximum value we can achieve in the present numerical simulations. The variation of the Weissenberg number representing the ratio of the elastic to

viscous stresses in the flow defined as ($Wi \equiv \lambda \dot{\varepsilon}$) at the central stagnation point with the flow Deborah number for geometries with sharp and round corners are presented in Figure 8 (b). Comparison with data from [Poole et al (2007)] for the sharp corner geometry exhibits a very good agreement. In particular, for values of $De < De_{cr}$ the local Weissenberg number increases with increasing Deborah number for geometries with sharp and round corners with the round corner geometry exhibiting slightly lower values of *Wi*. Beyond the critical *De* which is different for round and sharp corners, *Wi* decreases rather drastically with increasing *De* for the sharp corner geometry but only mildly for the round corner geometry; which can be explained by the fact that the flow asymmetry is less pronounced for the round corner geometry.

It is well known that the steady state extensional viscosity for the UCM model becomes unbounded when $\lambda \dot{\varepsilon} \to 1/2$ [Owens and Phillips (2002)]. In this flow, the Weissenberg number at the stagnation point exceeds the critical value of 0.5 before the asymmetry appears and consequently the streamwise normal stress at this point becomes unbounded. In [Poole et al (2007)] for the same geometry and flow, it is shown that the value of $\lambda \dot{\varepsilon}$ exceeds 0.5 at the geometric center of the cross slot or in other words the stress field becomes unbounded locally. The center is a stagnation point, and consequently the residence time is infinite and hence the steady state extensional viscosity is achieved, which for UCM model becomes unbounded at $\lambda \dot{\varepsilon} \geq 0.5$. It is to be noted that unbounded stress fields can also be present in a contraction flow even for Newtonian fluids, [Moffatt (1964)]. However, it is not the unbounded nature of the normal stress at the stagnation point that drives this instability [Poole et al (2007)] and this particular feature has also been observed with constitutive models that have bounded extensional viscosities, such as the FENE-P and FENE-CR models used by [Rocha et al (2009)].

For the cross-slot with round corners, Figure 9 presents the flow streamlines superimposed upon contours of the normalized first normal-stress difference for Newtonian and non-Newtonian fluid flows at increasing *De* and based on the asymmetric mesh with 10176 elements.

For the Newtonian and the non-Newtonian flows with $De < 0.38$ the flow remains symmetric, whereas at $De = 0.38$ asymmetric flow appears but confined to the central region of the cross-slot. This local flow asymmetry grows in extent at increasingly larger Deborah numbers up to the maximum value of computed flow ($De = 0.65$), as shown in Figure 9, but outside this central region the flow remains symmetric and this is well shown through the non-dimensional parameter *DQ*, which remains equal to zero, an indication of symmetry in terms of flow rate. The corresponding contour plots of $(\tau_{yy}\text{-}\tau_{xx})/(\eta U/H)$ remain symmetric outside the central region of the cross-slot, but show increasing values of the first normal stress differ-
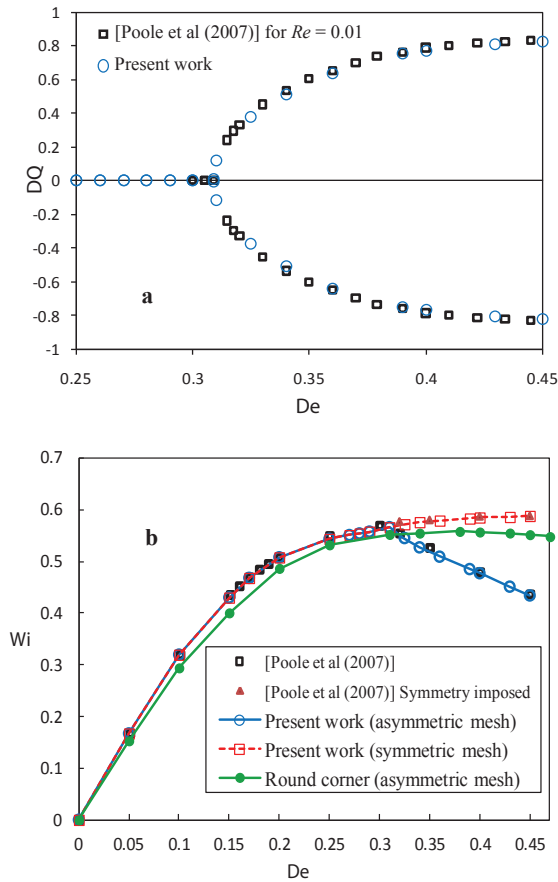
Figure 8: Influence of *De* on (a) the asymmetric parameter *DQ* and (b) *Wi* calculated at the stagnation point for sharp and round corner geometries at *Re* = 0.01 and comparison with numerical results of Poole et al. [10] for *Re* = 0 for the sharp corner geometry.

ence, especially in the stagnation point and around the rounded corners where the stress gradients are very large.

It is clear from these results that rounding the corners of the cross-slot inhibits the large stress gradients at the corners, when compared with the sharp corner cross-slot, and that this affects the flow behavior and in particular the critical Deborah numbers for the prediction of the flow asymmetry and for the variation of the non-dimensional parameter *DQ*.
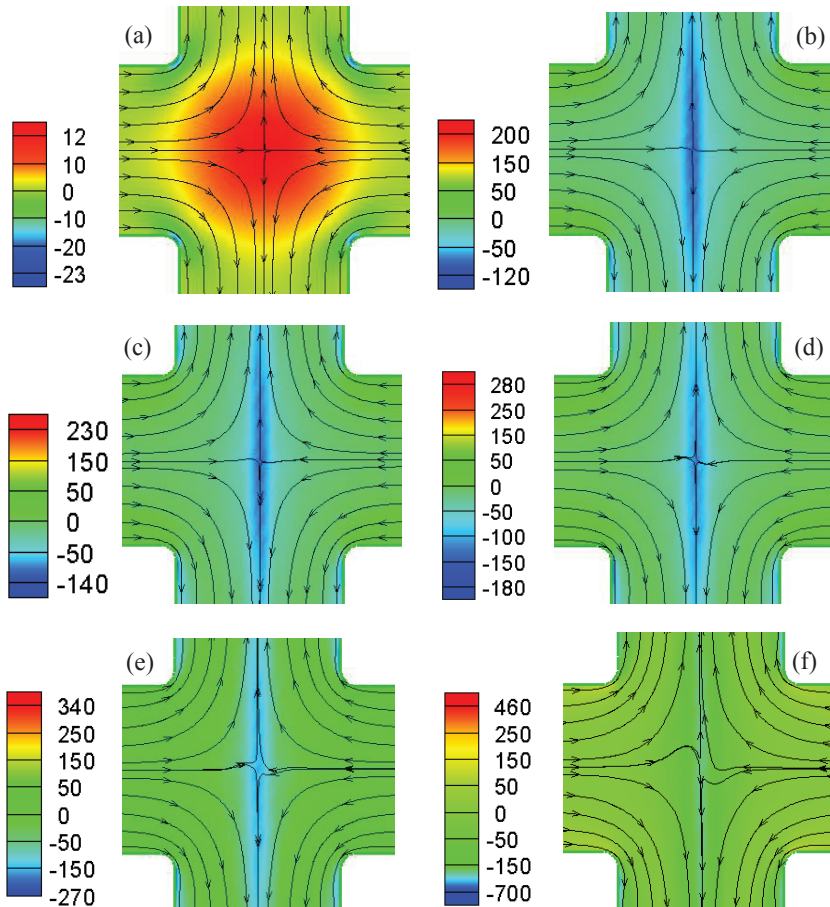
Figure 9:   Streamlines patterns superimposed onto contour plots of $(\tau_{yy}-\tau_{xx})/(\eta U/H)$ for the round corner cross-slot mapped with an asymmetric mesh: (a) $De = 0$ (Newtonian); (b) $De = 0.31$; (c) $De = 0.34$; (d) $De = 0.38$; (e) $De = 0.45$; (f) $De = 0.65$.

4.3   Inertial effects

The previous results all pertain to creeping flow conditions ($Re \approx 0$) and in this section we investigate the effect of inertia on the onset of flow asymmetry up to $Re = 3$. The *De-Re* stability map of Figure 10 compares our numerical results with those of [Poole et al (2007)] and confirms their earlier finding that inertia stabilizes the flow by increasing the critical Deborah number for transition to asymmetric

flow. Their results also showed that the stabilizing effect of inertia is accompanied with a reduction of the magnitude of the flow asymmetry. Our calculations in Figure 10 also indicate that the flow is slightly less stable than originally predicted by [Poole et al (2007)] since the present values of De_{cr} are lower at the same Reynolds number, except for the creeping flow limit, which was explored in more detail.
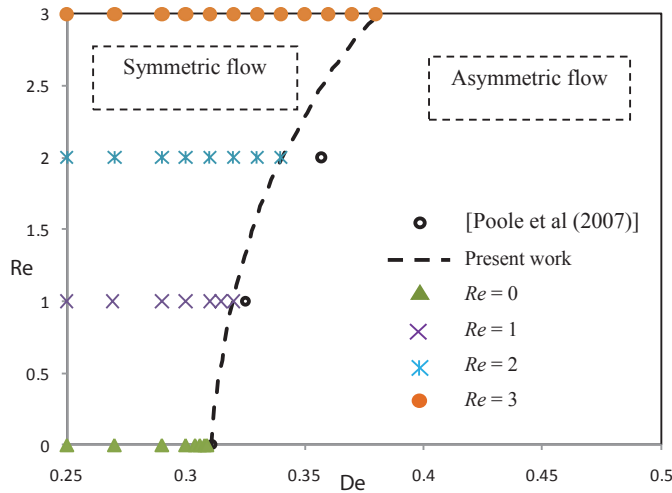
Figure 10: Effect of inertia on the critical Deborah number for the asymmetric flow in the sharp corner cross-slot.

5   Conclusions

The flow of viscoelastic fluids in planar cross-slot geometries with sharp and round corners has been investigated for creeping and low Reynolds number flow conditions. A finite element method was used for the first time in the present simulations, based on the UCM constitutive equation for the extra-stress tensor and a direct steady solver. Several poorly known aspects of this flow have been shown and previous results obtained with different methods have been confirmed.

The main conclusions from this work can thus be summarized as follows:

- When using a direct solver and the DEVSS/SU technique, asymmetric flow can be predicted with an asymmetric mesh whereas and the flow remains symmetric with a symmetric mesh.Therefore, the use of a proper mesh is a crucial factor in the process leading to the correct simulation of reality.

- Elasticity was seen to directly drive the instability: the Newtonian and non-Newtonian flows for De below the critical Deborah numbers ($De_{cr} = 0.309$ for the sharp corners geometry and $De_{cr} = 0.38$ for the round corners geometry) generate a symmetric flow, while for values above De_{cr} the flow becomes asymmetric but remains steady. In this physical system the asymmetric state is driven by the large normal stresses near the stagnation point and in the re-entrant corners of the cross-slot.

- Rounding the corners leads to an increase of the critical Deborah number, which for this particular radius of curvature ($R/H=0.1$) is $De_{cr} = 0.38$ (for sharp corners $De_{cr} = 0.309$). Additionally, the asymmetric flow is rather mild and was only observed in the central region near the stagnation point, without impacting the flow rate distribution through the outlets, which remained symmetric.

- Inertia was seen to stabilize the flow and the critical Deborah number increases with Re from $De_{cr} = 0.309$ for $Re \approx 0$ to $De_{cr} = 0.38$ for $Re = 3$. Beyond $Re = 3$ convergence problems were found for asymmetric flows.

The UCM constitutive model used in this work is only a crude approximation of real fluids, although exhibiting an unbounded extensional viscosity. Future work should aim to explore other constitutive models that are capable to describe other fluid features, like shear-thinning of the viscosity and bounded normal stresses, such as the Giesekus, FENE-P, Phan-Thien-Tanner and Pom-Pom models, among others.

Acknowledgement

References

Afonso, A. M.; Alves, M. A.; Pinho, F. T. (2010): Purely elastic instabilities in three-dimensional cross slot geometries. *J. Non-Newtonian Fluid Mech.* vol. 165, pp. 743-751.

Anna, S. L.; Bontoux, N.; Stone, H. A. (2003): Formation of dispersions using "flow focusing" in microchannels. *Appl. Phys. Let.,* vol. 82, pp. 364-366.

Arratia, P. E.; Thomas, C. C.; Diorio, J.; Gollub, J. P. (2006): Elastic instabilities of polymer solutions in cross-channel flow. *Physical Review Letters.,* vol. 96,

No. 144502.

Bird, R. B.; Dotson, P. J.; Johnson, N. L. (1980): Polymer solution rheology based on a finitely extensible bead-spring chain model. *J. Non-Newtonian Fluid Mech.* vol. 7, pp. 213-235.

Bird, R. B.; Hassager, O.; Armstrong, R. C.; Curtiss, C. F. (1987): Dynamics of Polymeric Liquids, Kinetic Theory. *John Wiley, New York.* vol. 2.

Chilcott, M. D.; Rallison, J. M. (1988): Creeping flow of dilute polymer solutions past cylinders and spheres. *J. Non-Newtonian Fluid Mech.,* vol. 29, pp. 381-432.

Dupret, F.; Marchal, J. M. (1986): Loss of evolution in the flow of viscoelastic fluids. *J. Non-Newtonian Fluid Mech.,* vol. 20, pp. 143-171.

Dylla-Spears, R.; Townsend, J. E.; Jen-Jacobson, L.; Sohn, L. L.; Muller, S. J. (2010): Single-molecule sequence detection via microfluidic planar extensional flow at a stagnation point. *Lab Chip*, vol. 10, pp. 1543-1549.

Giesekus, H. (1966): On the stability of flow of viscoelastic fluids I. *Rheol. Acta,* vol. 5, pp. 239-252.

Guénette, R.; Fortin, M. (1995): A new mixed finite element method for computing viscoelastic flows. *J. Non-Newtonian Fluid Mech.*, vol. 60, pp. 27–52.

Haward, S. J.; Oliveira, M. S. N.; Alves, M. A.; McKinley, G. H. (2012): Optimized cross-slot flow geometry for microfluidic extensional rheometry. *Physical Review Letters,* vol. 109, No. 128301.

Keunings, R. (1986): On the high Weissenberg number problem. *J. Non-Newtonian. Fluid Mech.,* vol. 20, pp. 209–226.

Larson, R. G.; Shaqfeh, E. S. G.; Muller, S. J. (1990): A purely elastic instability in Taylor Couette flow. *J. Fluid Mech.,* vol. 218, pp. 573 - 600.

Moffatt, H.K. (1964): Viscous and resistive eddies near a sharp corner, *J. Fluid Mech.*, vol. 18, pp. 1–18.

Odell, J. A., Carrington, S. P. (2006): Extensional flow oscillatory rheometry. *J. Non-Newtonian Fluid Mech.,* vol. 137, pp. 110-120.

Oliveira, M. S. N.; Pinho, F. T.; Poole, R. J.; Oliveira, P. J.; Alves, M. A. (2009): Purely elastic flow asymmetries in flow-focusing devices. *J. Non-Newtonian Fluid Mech.*, vol. 160, pp. 31-39.

Oliveira, P. J.; Pinho, F. T.; Pinto, G. A. (1998): Numerical simulation of nonlinear elastic flows with general collocated finite-volume method. *J. Non-Newtonian Fluid Mech.*, vol. 79, pp. 1-43.

Owens, R. G.; Phillips, T. N. (2002): *Computational Rheology*. Imperial College Press; River Edge, NJ: Distributed by World Scientific Pub. Co.

Poole, R. J. Alves, M. A. Oliveira, P. J. (2007): Purely-elastic flow asymmetries. *Physical Review Letters.,* vol. 99, No. 164503.

Rajagopalan, D.; Armstrong, R.; Brown, R. A. (1990): Finite element methods for calculation of steady viscoelastic flow using constitutive equations with a Newtonian viscosity. *J. Non-Newtonian Fluid Mech.* vol. 39, pp. 159-192.

Remmelgas, J.; Singh, P.; Leal, L. G. (1999): Computational studies of nonlinear dumbbell models of Boger fluids in a cross-slot flow. *J. Non-Newtonian Fluid Mech.* vol. 88, pp. 31-61.

Rocha, G. N.; Poole, R. J.; Alves, M. A.; Oliveira, P J. (2009): On extensibility effects in the cross-slot flow bifurcation. *J. Non-Newtonian Fluid Mech.,* vol. 156, pp. 58-69.

Singh, P.; Leal, L. G. (1995): Finite element simulation of flow around a 3pi/2 corner using the FENE dumbbell model. *J. Non-Newtonian Fluid Mech.* vol. 58, pp. 279-313.

Notation

D	deformation rate tensor (s^{-1})
De	Deborah number ($\lambda U/H$)
De_{cr}	critical Deborah number
DQ	degree of flow asymmetry parameter, $DQ = (Q_2 - Q_1)/(Q_1 + Q_2)$
H	channel width (m)
Nx	number of cells along the *x*-direction
Ny	number of cells along the *y*-direction
N1	number of cells along the *x*- or *y*-direction
N2	number of cells along orthogonal- direction
Q	the total flow rate per unit depth supplied to each inlet channel (m^2/s)
Q_1, Q_2	the upper and the lower partial flow rates per unit depth supplied to each outlet channel (m^2/s)
R	radius of curvature of the rounded corners (m)
T	extra-stress tensor (Pa)
TNC	Total Number of Cells
TNE	Total Number of Elements
U	average velocity (m/s)
u	velocity vector (m/s)
Wi	Weissenberg number ($\equiv \lambda \dot{\varepsilon}$)
x, y	Cartesian coordinates (m)

Greek letters

λ	relaxation time (s)
$\dot{\varepsilon}$	strain rate (s^{-1})
τ_{xx}, τ_{xy}	normal and shear stresses (Pa)
η	viscosity coefficient of UCM model (Pa.s)